

Comprehensive landscape and simple rules for transition-metal Heusler semiconductors

Yubo Zhang^{1,*}, Zirui Dong^{2,*}, and Jun Luo^{3,*}

¹*Minjiang Collaborative Center for Theoretical Physics, College of Physics and Electronic Information Engineering, Minjiang University, Fuzhou 350108, China*

²*School of Materials Science and Engineering, Shanghai University, Shanghai 200444, China*

³*Interdisciplinary Materials Research Center, School of Materials Science and Engineering, Tongji University, Shanghai 201804, China*

*Corresponding email: yubo.drzhang@mju.edu.cn, ziruidong@shu.edu.cn, junluo@tongji.edu.cn

Heusler alloys, renowned for their multifunctionality and capacity for vast elemental customization, are primarily classified into half-Heusler (XYZ) and full-Heusler (X_2YZ) structural types. Typically, the 18-electron half-Heusler and the 24-electron full-Heusler alloys are recognized as semiconductors, following the Slater-Pauling rule. Semiconductors are desired for many applications, but they represent a minor portion compared to the predominantly metallic and half-metallic members of the Heusler family. To broaden the scope of Heusler semiconductors, advancements have been made in developing variants such as *double-half Heuslers* $XX'Y_2Z_2$ and *quaternary full Heuslers* $XX'YZ$, which incorporate four constituent elements. Recently, *vacancy-filling off-stoichiometric Heuslers* of ternary $X_{1+\beta}YZ$ ($0 \leq \beta \leq 1$) and quaternary $X_\alpha X'_\beta YZ$ ($1 \leq \alpha + \beta \leq 2$) have emerged as a more versatile strategy. However, the flexibility associated with off-stoichiometry inevitably leads to complications, including issues with fractional filling ratios and complex site occupations. This work presents a comprehensive landscape of transition-metal-containing Heusler semiconductors, focusing on the off-stoichiometric Heuslers but seamlessly encompassing the integer-stoichiometric systems. The structural and electronic properties can be theoretically understood through a few simple rules. Many systems have been experimentally validated, showcasing their potential for applications such as thermoelectric converters.

1. Introduction

Heusler alloys [1] are traditionally categorized into two main structural types for ternary systems, i.e., half-Heusler (XYZ) and full-Heusler (X_2YZ), with integer stoichiometries of 1:1:1 and 2:1:1, respectively. In transition-metal Heuslers, following the nomenclature by pioneering work of Galanakis [2-4], X represents high-valent elements (e.g., Fe, Co, and Ni) and is more electronegative, Y is a low-valent transition-metal element (e.g., Ti and V) and is more electropositive, while Z represents a main-group element with *sp* valence electrons (e.g., Al, Si, and Sb). The half-Heusler structure is composed of three interpenetrating face-centered-cubic sublattices occupied by X, Y, and Z elements, whereas the full-Heusler features a fourth sublattice occupied by an additional X. In half-Heuslers (Figure 1a), the Z and Y elements occupy respectively the 4a and 4d Wyckoff positions, forming a rock-salt framework through ionic-like bonds. The electronegative X elements enter the 4c interstitial positions, having strong covalent interactions with Y and Z elements, their nearest neighbors. In X_2YZ full-Heuslers (Figure 1a), both the 4c and 4d sites are filled by X, leading to a symmetrized structure at the 8c sites. The X-X chemical hybridization, although involving the second-nearest neighbors, is crucial for understanding the magnetic and electronic properties of the full-Heuslers [3]. The quaternary variant $XX'YZ$, in which X and X' represent two inequivalent elements, adheres to the integer stoichiometry of 1:1:1:1.

Thousands of Heusler alloys can be obtained through flexible elemental substitution, and their fundamental magnetic and electrical properties generally adhere to the well-known Slater-Pauling rule [5,6]. Typically, half-Heuslers with $N_t = 18$ valence electrons (per formula unit) are nonmagnetic semiconductors (e.g., CoTiSb and NiTiSn), while other electron counts lead to ferromagnetic half-metals with a net magnetization of $M_t = N_t - 18$ [2]. The corresponding rule for full-

Heuslers is $M_t = N_t - 24$ [3], where 24 electrons result in semiconductors (e.g., Fe_2VAl). This rule has been generalized to quaternary full Heuslers, such as *inverse Heuslers* [4] and *LiMgPdSn-type Heuslers* [7]. Assisted by the Slater-Pauling rule, researchers have identified some exotic materials beyond conventional nonmagnetic semiconductors, including ferromagnetic semiconductors, fully-spin-compensated ferrimagnetic semiconductors, spin-gapless semiconductors, half-metallic antiferromagnets, and topological insulators [8-10].

Semiconducting Heuslers, though critical for various applications like thermoelectrics, represent only a tiny fraction of the predominantly metallic and half-metallic Heusler family. Many efforts have been made to transform the 17- and 19-electron metallic half-Heuslers into 18-electron semiconductors. Anand et al. have theoretically proposed the *double-half-Heusler* concept that adheres to the conventional 18-electron rule by combining a 17-electron TiFeSb with a 19-electron TiNiSb , leading to an *averaged* material of $\text{Ti}_2\text{FeNiSb}_2$ or $\text{TiFe}_{0.5}\text{Ni}_{0.5}\text{Sb}$ [11,12]. In this material, the high-valent Fe and Ni elements mix and occupy the 4c sites, allowing $\text{TiFe}_{0.5}\text{Ni}_{0.5}\text{Sb}$ to conform to the half-Heusler structure. Similarly, occupation mixing can also occur at the 4b sites among the low-valent elements. An example is $\text{Mg}_{1-x}\text{Ti}_x\text{NiSb}$, whose endpoints are the 17-electron MgNiSb and 19-electron TiNiSb . The $\text{Mg}_{0.5}\text{Ti}_{0.5}\text{NiSb}$ alloy is a semiconductor with 18 electrons [13]. For the 19-electron half-Heusler, a more straightforward approach involves reducing one electron through vacancies: Zhu et al. introduced 20% vacancies onto Nb's sites (Y atom at 4b sites) in NbCoSb , resulting in the 18-electron $\text{Nb}_{0.8}\text{CoSb}$ [14,15]. Similarly, the 17-electron half-Heusler can absorb an additional electron to achieve the 18-electron configuration. Wolverton et al. utilized lithium as the electron donor, and they theoretically realized quaternary Heuslers belonging to the LiMgPdSn-type [16]. Other quaternary semiconductors with either 18 or 24 valence electrons have been recently identified from brute-force screening [17]. Note that the first three example materials (i.e., $\text{TiFe}_{0.5}\text{Ni}_{0.5}\text{Sb}$, $\text{Mg}_{0.5}\text{Ti}_{0.5}\text{NiSb}$, $\text{Nb}_{0.8}\text{CoSb}$) still belong to the half-Heusler category despite their non-stoichiometric appearance, which is distinct from the vacancy-filling off-stoichiometric Heuslers to be discussed later.

Vacancy-filling off-stoichiometric Heuslers (Figure 1a), which eschew the constraints of integer stoichiometry, have emerged as a more versatile strategy for realizing semiconducting behaviors. Instead of compromising the integrity of the rock-salt framework, this approach focuses on engineering the filling of interstitial vacancy sites, aiming for an occupation ratio intermediate between half- and full-Heuslers. For example, ternary $\text{X}_{1+\beta}\text{YZ}$ (with $0 < \beta < 1$) represents the fractional vacancy filling ratio, and the half- and full-Heuslers are recovered at the endpoints (i.e., $\beta = 0$ and $\beta = 1$). $\text{Fe}_{1.5}\text{TiSb}$ was the first system theoretically predicted in 2016 [18], although experiments revealed poor-quality samples that exhibited significant defects and secondary metallic phases [18,19]. The bandgap mechanism of $\text{Fe}_{1.5}\text{TiSb}$ was later detailed by Snyder and colleagues [20], a topic we will revisit in this work.

Our team has worked extensively on these materials in recent years. For instance, we synthesized a similar material, $\text{ZrRu}_{1.5}\text{Sb}$, which exhibits clear semiconductor behaviors [21]. We also found that $\text{TiRu}_{1+x}\text{Sb}$ displays semiconductor or near-semiconductor properties across various compositions [22]. Additionally, we designed and realized the quaternary $\text{TiFe}_x\text{Cu}_y\text{Sb}$, which transits from good to poor semiconductors by varying the composition [23]. We observed exotic behaviors such as non-Fermi-liquid behavior in $\text{TiFe}_{1.33}\text{Sb}$ [19] and Kondo-like magnetic phenomena in Cr-doped $\text{Nb}_{0.75}\text{Ti}_{0.25}\text{FeSb}$ [24], both deviating slightly from the optimal semiconducting stoichiometries.

While the *vacancy-filling* strategy significantly expands the range of Heusler semiconductors, it also poses substantial challenges in understanding the materials associated with the off-stoichiometry. Moreover, many new candidates have yet to be explored. This work presents a comprehensive landscape of Heusler semiconductors, focusing on systems containing transition-metal elements. As we explore the off-stoichiometric formulations, the resulting landscape naturally includes the integer-stoichiometric formulations as exceptional cases. Simple rules are proposed to understand the structural and electronic properties, and some materials are experimentally validated. Our findings may inspire further exploration and development of these materials.

2. Simplified understanding of the bandgap mechanisms

Before addressing the bandgap mechanism, we categorize the Heusler compounds based on their composition and stoichiometry. As depicted in Figure 1b, the general formula can be expressed as $X_\alpha^{4c}X'_\beta^{4d}Y^{4b}Z^{4a}$ (X and X' are high-valent transition-metal elements), with the 4c-4d interstitial occupations following a constrain of $1 \leq \alpha + \beta \leq 2$. The familiar integer-stoichiometric Heuslers include XYZ for the *ternary half-Heusler* (THH) and X_2YZ for the *ternary full-Heusler* (TFH). *Quaternary half-Heusler* (QHH) is expressed as $X_\alpha X'_{1-\alpha}YZ$, including the intermediate $X_{0.5}X'_{0.5}YZ$ for the double-half Heusler [11]. *Quaternary full-Heusler* (QFH) is expressed as $X_\alpha X'_{2-\alpha}YZ$, where $XX'YZ$ represents the well-studied quaternary Heusler. We use $X_{1+\beta}YZ$ to represent the *ternary off-stoichiometric Heusler* (TOSH) and $X_\alpha X'_\beta YZ$ for the *quaternary off-stoichiometric Heusler* (QOSH). The objective of this work is to determine the filling coefficients that lead to a semiconducting phase, characterized by specific electron counts and atomic occupation patterns.

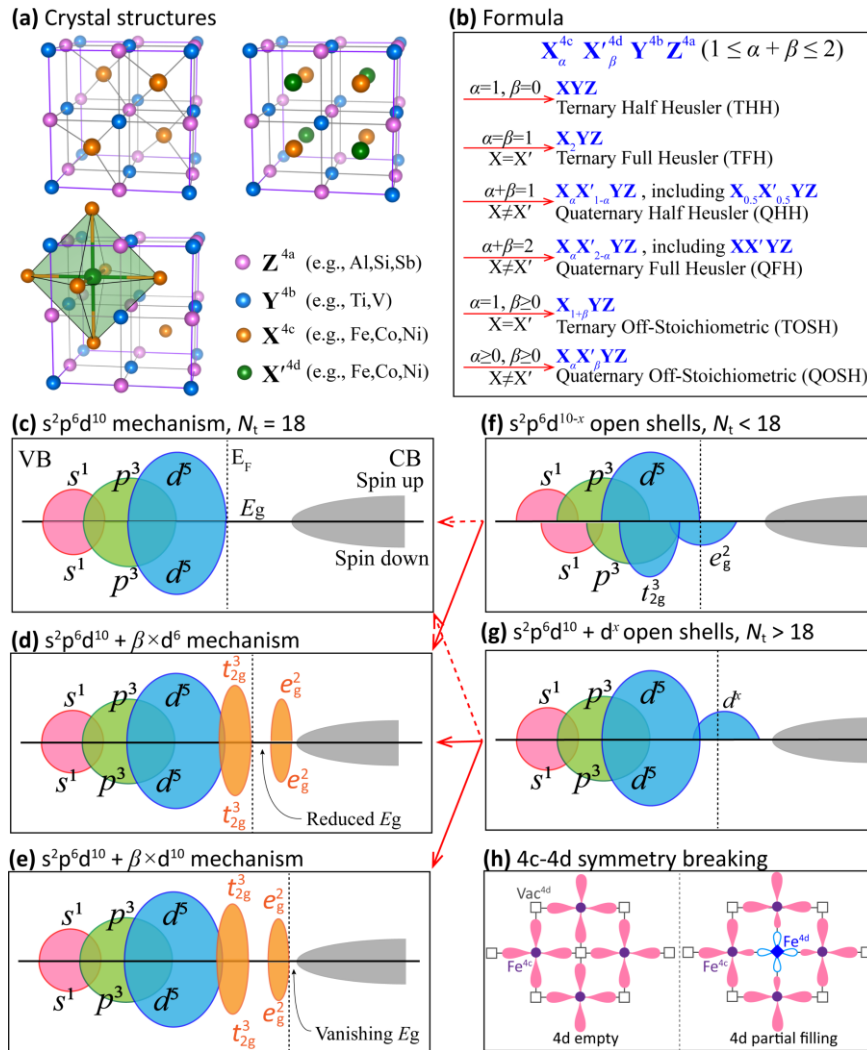


Figure 1. Simplified gapping scenarios in transition-metal Heusler semiconductors. (a) Crystal structures of half-, full-, and vacancy-filling off-stoichiometric Heuslers. In the last structure, an octahedron is plotted to highlight the interaction between 4c and 4d sites. (b) Categorization of Heusler materials. (c) A cartoon plot illustrates the electronic density-of-states and the $s^2p^6d^{10}$ bandgap mechanism of 18-electron semiconductors. (d) Bandgap formation due to $t_{2g}-e_g$ octahedral field splitting leads to an $s^2p^6d^{10} + \beta \times d^6$ mechanism. (e) Bandgap mechanism of $s^2p^6d^{10} + \beta \times d^{10}$. (f, g) Metallic Heuslers with open d -shells. (h) Breaking of 4c-4d geometrical symmetry in off-stoichiometric Heuslers due to the 4d orbitals experiencing more next-neighboring repulsions than the 4c orbitals. Solid lines between subplots denote bandgap strategies via vacancy-filling, whereas dashed lines illustrate alternative strategy.

Heusler's bandgap is intricately linked to the formation of fully occupied hybrid orbitals through covalent bonding interaction, and the mechanisms in THH and TFH have been detailed using orbital hybridization diagrams [2,3]. Figure 1c

schematically shows the $s^2p^6d^{10}$ hybrid orbitals for THH $X^{4c}Y^{4b}Z^{4a}$, where the bandgap is above the occupied orbitals. When XYZ has fewer than 18 electrons ($N_t < 18$, see Figure 1f), the spin-down d -shells are incomplete, resulting in half-metallicity and net magnetization. To compensate for the electron deficiency in XYZ, the *vacancy-filling strategy* introduces a fraction of X transition-metal atoms into the 4d interstitial sites, resulting in the chemical formula $X^{4c}Y^{4b}Z^{4a}+X_\beta^{4d}$ or equivalently $X_{1+\beta}YZ$ ($0 \leq \beta \leq 1$). The transition from Figure 1f to 1c, which is conceptually straightforward and has been utilized in lithium-doped systems [16], is unrealistic for the vacancy-filling approach based on transition-metal elements. The reason is that the transition-metal ion at the 4d sites—typically high-valent transition metals—tends to retain some d electrons as valence electrons; but, low-valent transition metals are usually too electropositive to occupy interstitial sites [9]. These 4d-site elements, after donating electrons to the XYZ framework, must also create *local gaps* to render the entire structure insulating. The gapping mechanism is termed as $s^2p^6d^{10}+\beta \times d^6$ (Figure 1d): the inserted 4d ion experiences Coulombic repulsion from six neighboring 4c ions (Figure 1h), leading to octahedral crystal-field splitting between t_{2g} and e_g orbitals. Although the 4c and 4d sites are next-neighboring, their d -orbitals interaction can be significant due to the directional nature of the e_g orbitals [3]. This mechanism applies to the TOSH $Fe_{1.5}TiSb$ [18,20] and $Ru_{1.5}ZrSb$ [21].

When XYZ has more than 18 electrons ($N_t > 18$, see Figure 1g), three mechanisms can potentially open a bandgap. The first approach involves reverting XYZ to the 18-electron configuration by removing excess electrons (from Figure 1g to 1c). The aforementioned $Nb_{0.8}CoSb$ belongs to this category [14,15]. The second approach is to transform Figure 1g to 1d via vacancy filling, but it is practically challenging due to the unique electronic characteristics of the transition-metal elements, as detailed in the [Supplementary Materials](#). A more promising approach is termed $s^2p^6d^{10}+\beta \times d^{10}$ mechanism (Figure 1e) associated with vacancy filling. In this scenario, the doped 4d atoms initially absorb excess electrons from the $X^{4c}Y^{4b}Z^{4a}$ matrix, leaving 18 electrons; subsequently, the resulting 4d ions can develop local gaps if their d -shells become fully filled. Practically, the doped X' element must be different from the X element in the host, leading to QOSH $X^{4c}Y^{4b}Z^{4a}+X'\beta^{4d}$.

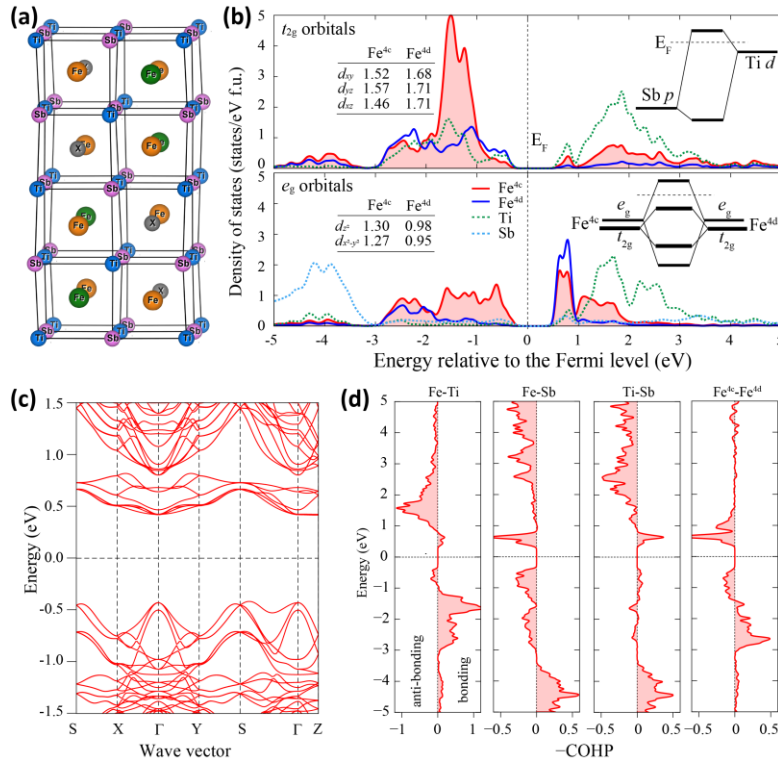


Figure 2. Bandgap formation in $Fe_{1.5}TiSb$. (a) Structural model. (b) Electronic density-of-states for one $Fe_{1.5}TiSb$ formula, containing one Fe^{4c} atom and a half Fe^{4d} atom. The electron numbers in the inset are in units of electrons per orbital. The insets also show the dominant orbital interactions, inspired by Ref. [3]. (c) Band structure. (d) Bonding and

antibonding interactions characterized by Crystal Orbital Hamilton Population (COHP). Four pair interactions are considered: Fe- d with Ti- d , Fe- d with Sb- p , Ti- d with Sb- p , and Fe^{4c}- d with Fe^{4d}- d orbitals.

While the $s^2p^6d^{10}+\beta\times d^{10}$ mechanism is clear and straightforward, the $s^2p^6d^{10}+\beta\times d^6$ mechanism warrants further explanation, as exemplified in Fe_{1.5}TiSb (Figure 2). We have interpreted the $s^2p^6d^{10}+\beta\times d^6$ mechanism as "full- t_{2g} and empty- e_g " orbital configurations. Applying this interpretation to Fe_{1.5}TiSb would suggest nominal orbital configurations of Fe^{4c}- d^{10} and Fe^{4d}- d^6 , indicating the presence of distinct species of (Fe^{4c})²⁺ and (Fe^{4d})²⁻ [20]. However, the calculated electronic density of states (Figure 2b) reveals stark contradictions. First, the integrated electron numbers for Fe^{4c} and Fe^{4d} ions are nearly identical, at 7.13 and 7.02 electrons, respectively. Second, the Fe^{4d}- e_g orbitals retain a considerable number of electrons (approximately 1.93 electrons per atom) instead of presenting an empty configuration. These inconsistencies imply that the t_{2g} - e_g splitting in an octahedral field (Figure 1a) is an oversimplification for Fe_{1.5}TiSb, though conceptually simple and useful.

In Fe_{1.5}TiSb, the atomic interactions include nearest-neighbor Fe-Ti and Fe-Sb forming tetrahedrons as well as second-nearest Ti-Sb and Fe^{4d}-Fe^{4c} forming octahedrons (Figure 2d). It is the Fe^{4d}-Fe^{4c} interaction that introduces the *local gaps* and distinguishes the vacancy-containing Heuslers from the half-Heuslers. For comparison, we start by analyzing the Ti-Sb interactions, where hybridization between Ti- e_g orbitals and Sb- p orbitals leads to lower-energy bonding states and higher-energy antibonding states (see the inset of Figure 2b). The bonding (antibonding) states are predominantly derived from Sb- p (Ti- e_g) orbitals because the Sb- p is considerably lower in energy. By contrast, the Fe^{4c}- d and Fe^{4d}- d atomic orbitals, which energetically degenerate before hybridization, contribute almost equally to the bonding and antibonding states. Moreover, the e_g - e_g orbital interaction is more pronounced than the t_{2g} - t_{2g} interaction due to the directional characteristics of the e_g orbitals, resulting in a local gap between two groups of antibonding states (see the inset of Figure 2b). Consequently, Fe- e_g orbitals are partially occupied, contrary to the empty scenario from the nominal valence [20]; Fe- t_{2g} orbitals are not fully occupied, as they also hybridize with Ti-3d orbitals at similar energy levels. We conclude that the fundamental bandgap mechanism in Fe_{1.5}TiSb mirrors that in integer-stoichiometric full-Heuslers [3]. However, the environmental differences at the Fe^{4c} and Fe^{4d} sites, i.e., e_g orbitals at the 4d sites face more neighboring repulsions than those at the 4c sites (Figure 1h), reducing 4d- e_g occupations to some extent. This is evidenced by the reduced electron counts in the Fe^{4d}- dz^2 (0.98) and dx^2-y^2 (0.95) orbitals compared to those in the Fe^{4c}- dz^2 (1.30) and dx^2-y^2 (1.27) orbitals.

3. Bandgap engineering and Electron number rules

After understanding the bandgap mechanisms, we demonstrate how to transform a metallic XYZ into a semiconducting XYZ+X'_β, which involves selecting the X' element and determining the filling coefficient β. Figure 3a starts with half-Heuslers with $N_t = 18$, which are semiconductors following the $s^2p^6d^{10}$ gapping mechanism. Most other XYZ systems are metals with either deficient electrons ($N_t = 14 \sim 17$) or excess electrons ($N_t = 19 \sim 20$). In the electron-deficient FeTiSb, for example, we apply the $s^2p^6d^{10}+\beta\times d^6$ mechanism by introducing a homo-element of Fe_β to the 4d sites. The process of determining the β coefficient in the targeted FeTiSb+Fe_β is shown in the inset of Figure 3b: The FeTiSb framework accepts one electron from the Fe_β atoms, achieving the 18-electron configuration. Since the Fe_β atoms originally possess 8β electrons, the remaining 8β - 1 electrons should fully fill the 4d- t_{2g} orbitals with six electrons, leading to 8β - 1 = 6 and β = 0.5.

Engineering on NiTiSb relies on the $s^2p^6d^{10}+\beta\times d^{10}$ mechanism since NiTiSb already contains one excess electron of more than 18. A hetero-element with lower valence, for example Fe, is introduced to the 4d sites to accommodate the excess electron. As shown in Figure 3c, the NiTiSb framework donates the excess electron to the Fe_β atoms, achieving the 18-electron configuration. The Fe_β atoms, now possessing 8β + 1 electrons, can create a *local gap* if all the d -orbitals are filled to a d^{10} configuration, resulting in 8β + 1 = 10 and β = 0.5.

Fe_αTiSb (0 < α < 1) represents a more generic formulation where the Fe atoms are insufficient to reach a half-Heusler concentration. It can be transformed into semiconductors when filling with Co atoms through the $s^2p^6d^{10}+\beta\times d^6$ mechanism, resulting in Fe_αTiSb+Co_β or equivalently (Fe_αCo_β)TiSb (Figure 3d). For conceptual simplicity, we assume the XYZ

framework is CoTiSb, leaving the other atoms (i.e., Fe_α and Co_{β-1}) to occupy the 4d sites. This arrangement creates 4d *local gaps* under the condition that $8\alpha + 9(\beta - 1) = 6(\alpha + \beta - 1)$, of which a pictorial explanation is provided in the [Supplementary Materials](#). The resulting relationship, $2\alpha + 3\beta = 3$, indicates that the compositions are continuously variable. [Figure 3e](#) also demonstrates an example of introducing the Cu element to Fe_αTiSb, revealing an interesting phenomenon in (Fe_αCu_β)TiSb: both gapping mechanisms are applicable and lead to two stoichiometry relations. For the $s^2p^6d^{10}+\beta\times d^6$ mechanism producing $2\alpha + 5\beta = 3$, all the Cu atoms enter 4c sites, while all the inserted atoms at 4d sites are entirely of Fe atoms. By contrast, all the Fe atoms enter 4c sites for the $s^2p^6d^{10}+\beta\times d^{10}$ mechanism, which gives $2\alpha - \beta = 1$. Such arrangements are governed by site occupation rules, to be discussed in [Section 5](#).

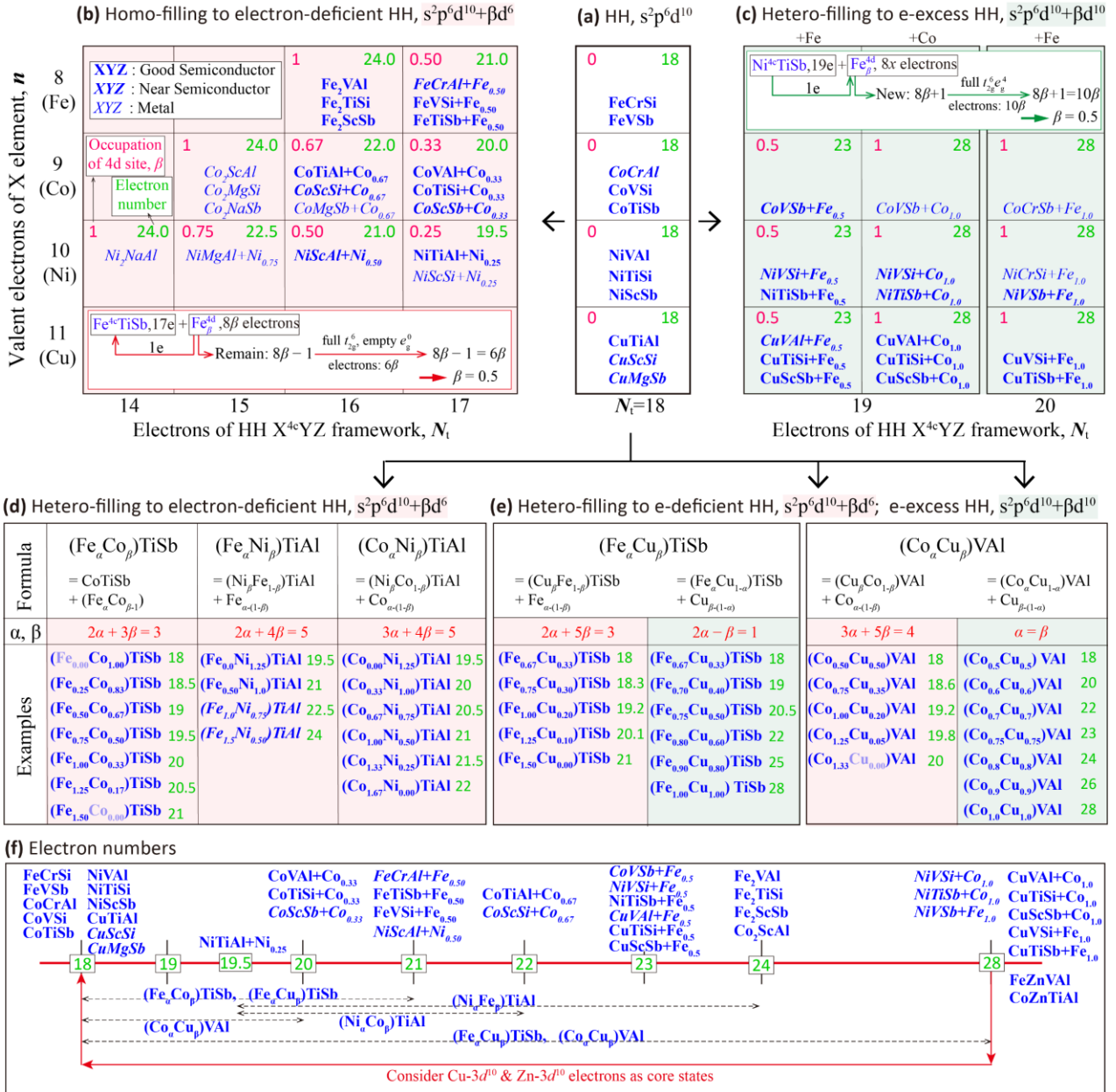


Figure 3. Heuslers and their transformation into semiconductors. (a) Half-Heuslers with 18 electrons. (b) Electron-deficient HH XYZ employs the $s^2p^6d^{10}+\beta\times d^6$ bandgap mechanism by filling the 4d sites with the homo-element X. (c) Electron-excess HH XYZ utilizes the $s^2p^6d^{10}+\beta\times d^{10}$ mechanism via filling the 4d sites with the hetero-element X'. (d) Hetero-filling of the electron-deficient half-Heuslers. In (Fe_αCo_β)TiSb, (Ni_αFe_β)TiAl, and (Ni_αCo_β)TiAl, the compositions change continuously. (e) Hetero-filling Cu-based systems implement both the $s^2p^6d^{10}+\beta\times d^6$ and $s^2p^6d^{10}+\beta\times d^{10}$ mechanisms. (f) Heusler semiconductors are categorized by their valence electron counts. Material formulas are styled in **bold** for those with a well-recognized bandgap in the simulation, in *bold italics* for near-semiconducting materials that represent either reality or theoretical misestimations, and in *thin italics* for those identified as metallic.

The bandgap mechanisms essentially fix the electron numbers, but the predicted systems may face practical constraints in developing a bandgap. We carry out examinations using density-functional theory, and some selected systems are further validated experimentally. According to the simulations, semiconductors (or near-semiconductors, considering the theoretical problem of bandgap underestimation) are particularly abundant in systems containing Fe, Co, Ni, and Cu (see Figures 3 and 4; also refer to the Supplementary Materials for the complete results). Experimentally, we have synthesized high-quality polycrystalline samples of a few systems, as shown in Figure 4b. Quaternary half-Heusler ($\text{Fe}_{0.67}\text{Cu}_{0.33}\text{TiSb}$) [23] adheres to the $s^2p^6d^{10}$ mechanism. The QOSH ($\text{FeCu}_{0.2}\text{TiSb}$) [25] relies on the $s^2p^6d^{10}+\beta\times d^6$ bandgap mechanism, while (FeCu)TiSb and ($\text{Fe}_{0.75}\text{Cu}_{0.50}\text{TiSb}$) [23] utilize the $s^2p^6d^{10}+\beta\times d^{10}$ mechanism. In addition, previous research [26] has investigated the thermoelectric properties of quinary Heusler materials, i.e., $(\text{Co}_{0.85}\text{Cu}_{0.65})\text{Zr}(\text{Sn}_{1-y}\text{Sb}_y)$ with $0 \leq y \leq 0.25$, and it is utilized to test our theoretical predictions. The X-ray diffraction patterns (Figure 4c) indicate that the samples with $0 \leq y \leq 0.2$ are high-quality single-phase crystals, whereas the sample with $y = 0.25$ displays a secondary phase. The endpoint ($\text{Co}_{0.85}\text{Cu}_{0.65}\text{Zr}(\text{Sn}_{0.8}\text{Sb}_{0.2})$) exhibits the lowest electrical conductivity and the highest Seebeck coefficient ($\sim 0.2 \times 10^5$ S/m and ~ 50 $\mu\text{V}/\text{K}$ at 300 K), suggesting that this sample closely approximates semiconductor behavior. Our theoretical simulations (Figure 4d) show that the samples with $y < 0.2$ behave as p -type metals, while the sample with $y = 0.2$ acts as an intrinsic semiconductor. ($\text{Co}_{0.85}\text{Cu}_{0.65}\text{Zr}(\text{Sn}_{0.8}\text{Sb}_{0.2})$) adheres to the $s^2p^6d^{10}+\beta\times d^{10}$ bandgap mechanism since the nominal orbital configurations are $\text{Co}-d^{10}$, $\text{Cu}-d^{10}$, $\text{Zr}-d^0$, $\text{Sn}-s^2p^6$, and $\text{Sb}-s^2p^6$. An even higher electron concentration at $y = 0.25$ results in n -type behavior, which explains the experimental difficulty in realizing a single phase.

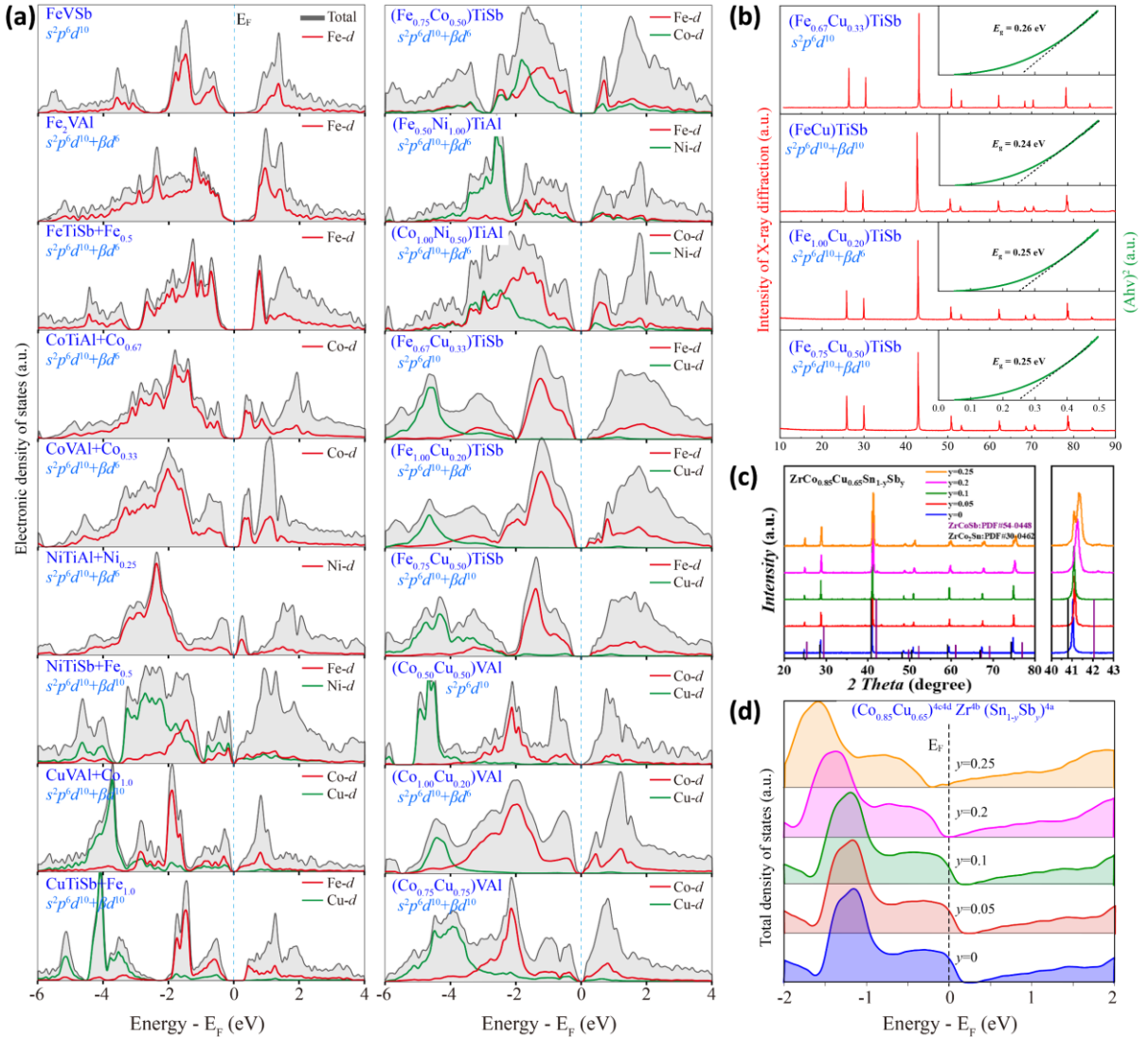


Figure 4. Characterization of selected Heusler semiconductors. (a) Electronic density-of-states. (b) Experimental X-ray diffraction (XRD) patterns of the $(\text{Fe}_a\text{Cu}_b)\text{TiSb}$ samples, with insets showing the determination of optical bandgaps.

(c) XRD of quinary $(\text{Co}_{0.85}\text{Cu}_{0.65})\text{Zr}(\text{Sn}_{1-y}\text{Sb}_y)$ with $0 \leq y \leq 0.25$. Note the double-peak structures for the $y = 0.25$ sample, indicating the presence of a secondary phase. (d) Evolution of density-of-states for the $(\text{Co}_{0.85}\text{Cu}_{0.65})\text{Zr}(\text{Sn}_{1-y}\text{Sb}_y)$ materials. Subplot (c) is reproduced from Ref. [26] with permission.

The predicted semiconductors can be organized according to their valence electron numbers, as shown in Figure 3f. Besides the well-known 18 electrons in THH and 24 in TFH, TOSH semiconductors exhibit a range of discrete electron counts including 19, 19.5, 20, 21, 22, 23, and 28. Furthermore, QOSH semiconductors continuously span the entire range from 18 to 28 electrons. This finding demonstrates that the vacancy-filling strategy significantly expands the family of semiconducting Heuslers. The 28-electron systems, classified as $\text{XX}'\text{YZ}$ QFH, warrant attention. The density-of-states analysis indicates that Cu-3d orbitals are consistently fully occupied and positioned deep away from the band edge (Figure 4). For example, the Cu-3d states in $\text{CuTiSb}+\text{Fe}_{1.0}$ are notably deeper than the higher-energy Fe-3d states. In $\text{CuVAI}+\text{Co}_{1.0}$, there is a slight overlap between Cu-3d and Co-3d orbitals, though it is minimal. From a theoretical standpoint, it is more consistent to include Cu-3d electrons in the valence electron count. By contrast, Zn-3d electrons are positioned even deeper than Cu-3d electrons (see Supplementary Materials), which justifies the flexibility of excluding them from the valence electron count. These analyses highlight the connection between 28-electron and 18-electron Heuslers materials.

4. Comprehensive landscape

Exploring the most generic formula for Heuslers, i.e., $\text{X}_\alpha\text{X}'_\beta\text{YZ}$ for QOSH, unveils a comprehensive landscape of semiconducting Heuslers, as depicted in Figure 5. This figure incorporates all the bandgap mechanisms— $s^2p^6d^{10}$, $s^2p^6d^{10}+\beta \times d^6$, and $s^2p^6d^{10}+\beta \times d^{10}$ —and covers both integer-stoichiometric and off-stoichiometric Heuslers. We discuss several intriguing trends. First, semiconductors derived from the $s^2p^6d^{10}+\beta \times d^6$ mechanism are more numerous than those from the $s^2p^6d^{10}+\beta \times d^{10}$ mechanism. In the former situation, e_g-e_g interaction [3] is typically significant (especially for larger ions), which ensures the ability to open a bandgap. In contrast, the latter mechanism initiates a bandgap atop the d^{10} orbitals. These systems often have densely populated electrons where mutual repulsion tends to minimize and eventually close the bandgap. Second, the landscape presents many new off-stoichiometric half- and full-Heuslers, which are particularly interesting and simpler regarding theoretical understanding and experimental realization. For QHH half-Heuslers, semiconductors or near-semiconductors include $\text{Fe}_{0.5}\text{Ni}_{0.5}\text{TiSb}$, $\text{Fe}_{0.33}\text{Cu}_{0.67}\text{VAI}$, $\text{Fe}_{0.67}\text{Cu}_{0.33}\text{TiSb}$, $\text{Co}_{0.5}\text{Cu}_{0.5}\text{VAI}$, $\text{Fe}_{0.25}\text{Zn}_{0.75}\text{TiAl}$, $\text{Fe}_{0.5}\text{Zn}_{0.5}\text{VAI}$, $\text{Fe}_{0.75}\text{Zn}_{0.25}\text{TiSb}$, $\text{Co}_{0.33}\text{Zn}_{0.67}\text{TiAl}$, and $\text{Co}_{0.67}\text{Zn}_{0.33}\text{VAI}$. QFH full-Heuslers contains $\text{Fe}_{1.5}\text{Ni}_{0.5}\text{TiAl}$, $\text{Fe}_{1.33}\text{Cu}_{0.67}\text{ScAl}$, $\text{Fe}_{1.67}\text{Cu}_{0.33}\text{TiAl}$, $\text{Fe}_{1.75}\text{Zn}_{0.25}\text{TiAl}$, $\text{Fe}_{0.5}\text{Ni}_{1.5}\text{TiAl}$, $\text{Fe}_{0.33}\text{Cu}_{1.67}\text{TiAl}$, $\text{Fe}_{0.67}\text{Cu}_{1.33}\text{VAI}$, $\text{Co}_{0.5}\text{Cu}_{0.5}\text{TiAl}$, $\text{Fe}_{0.75}\text{Zn}_{1.25}\text{TiAl}$, FeCuTiSb , FeZnVAI , CoCuVAI , and CoZnTiAl . The richness of Al-based semiconductors may be related to the particular energy of Al-3p orbitals [27]. More candidates are anticipated when substituting the 4a and 4b atoms [26]. Third, when using Ni as the filling element under the $s^2p^6d^{10}+\beta \times d^{10}$ mechanism, there are many systems without constraints on the filling fraction β [28]. For instance, $\text{Fe}_\alpha\text{TiSb}+\text{Ni}_\beta$ conforms to the relationship of $2\alpha = 1$, indicating that $\text{Fe}_{0.5}\text{TiSb}$ can accommodate Ni atoms in amounts ranging from $\beta = 0.5$ to 1.5 (due to the constrain of $1 \leq \alpha + \beta \leq 2$, instead of electron number consideration). While the full-Heusler $\text{Fe}_{0.5}\text{Ni}_{1.5}\text{TiSb}$ exhibits near-semiconductor behavior, systems with lower Ni concentrations (e.g., from $\text{Fe}_{0.5}\text{Ni}_{0.5}\text{TiSb}$ to $\text{Fe}_{0.5}\text{Ni}_{1.0}\text{TiSb}$) are good semiconductors (see Supplementary Materials). A similar phenomenon has been observed in $\text{FeNbSb}+\text{Cr}_\beta$ systems [24], where arbitrary additions of Cr atoms (having six valence electrons) consistently result in semiconductors following the $s^2p^6d^{10}+\beta \times d^6$ bandgap mechanism.

| YZ electrons | Mechanisms of $s^2p^6d^{10}$ and $s^2p^6d^{10}+\beta d^6$ | | | | Mechanism of $s^2p^6d^{10}+\beta d^{10}$ | | | |
|------------------------------------|---|---|--|--|---|--|---|--|
| | +Co $_{\beta}$ | +Ni $_{\beta}$ | +Cu $_{\beta}$ | +Zn $_{\beta}$ | +Co $_{\beta}$ | +Ni $_{\beta}$ | +Cu $_{\beta}$ | +Zn $_{\beta}$ |
| $N_{YZ} = 6$ e.g., Fe $_a$ ScAl | $2\alpha + 3\beta = 6$ <i>Co₂ScAl</i> | $2\alpha + 4\beta = 6$ <i>FeNiScAl</i> | $2\alpha + 5\beta = 6$ <i>Fe_{1.33}Cu_{0.67}ScAl</i> | $2\alpha + 6\beta = 6$ <i>ZnScAl</i> <i>Fe_{1.5}Zn_{0.5}ScAl</i> | $2\alpha + \beta = -2$ | $2\alpha = -2$ | $2\alpha - \beta = -2$ <i>Cu₂ScAl</i> | $2\alpha - 2\beta = -2$ <i>Fe_{0.5}Zn_{1.5}ScAl</i> |
| $N_{YZ} = 7$ e.g., Fe $_a$ TiAl | $2\alpha + 3\beta = 5$ <i>FeCoTiAl</i> | $2\alpha + 4\beta = 5$ <i>Fe_{1.5}Ni_{0.5}TiAl</i> | $2\alpha + 5\beta = 5$ <i>CuTiAl</i> <i>Fe_{1.67}Cu_{0.33}TiAl</i> | $2\alpha + 6\beta = 5$ <i>Fe_{0.25}Zn_{0.75}TiAl</i> <i>Fe_{1.75}Zn_{0.25}TiAl</i> | $2\alpha + \beta = -1$ | $2\alpha = -1$ | $2\alpha - \beta = -1$ <i>Fe_{0.33}Cu_{1.67}TiAl</i> | $2\alpha - 2\beta = -1$ <i>Fe_{0.75}Zn_{1.25}TiAl</i> |
| $N_{YZ} = 8$ e.g., Fe $_a$ VAl | $2\alpha + 3\beta = 4$ <i>Fe₂VAl</i> | $2\alpha + 4\beta = 4$ <i>NiVAl</i> <i>Fe₂VAl</i> | $2\alpha + 5\beta = 4$ <i>Fe_{0.33}Cu_{0.67}VAl</i> <i>Fe₂VAl</i> | $2\alpha + 6\beta = 4$ <i>Fe_{0.5}Zn_{0.5}VAl</i> <i>Fe₂VAl</i> | $2\alpha + \beta = 0$ | $2\alpha = 0$ <i>Ni₂VAl</i> | $2\alpha - \beta = 0$ <i>Fe_{0.67}Cu_{1.33}VAl</i> | $2\alpha - 2\beta = 0$ <i>FeZnVAl</i> |
| $N_{YZ} = 9$ e.g., Fe $_a$ TiSb | $2\alpha + 3\beta = 3$ <i>CoTiSb</i> | $2\alpha + 4\beta = 3$ <i>Fe_{0.5}Ni_{0.5}TiSb</i> | $2\alpha + 5\beta = 3$ <i>Fe_{0.67}Cu_{0.33}TiSb</i> | $2\alpha + 6\beta = 3$ <i>Fe_{0.75}Zn_{0.25}TiSb</i> | $2\alpha + \beta = 1$ | $2\alpha = 1$ <i>Fe_{0.5}Ni_{1.5}TiSb</i> | $2\alpha - \beta = 1$ <i>FeCuTiSb</i> | $2\alpha - 2\beta = 1$ <i>Fe_{1.25}Zn_{0.75}TiSb</i> |
| $N_{YZ} = 10$ e.g., Fe $_a$ VSb | $2\alpha + 3\beta = 2$ <i>FeVSb</i> | $2\alpha + 4\beta = 2$ <i>FeVSb</i> | $2\alpha + 5\beta = 2$ <i>FeVSb</i> | $2\alpha + 6\beta = 2$ <i>FeVSb</i> | $2\alpha + \beta = 2$ <i>Co₂VSb</i> | $2\alpha = 2$ <i>FeNiVSb</i> | $2\alpha - \beta = 2$ <i>Fe_{1.33}Cu_{0.67}VSb</i> | $2\alpha - 2\beta = 2$ <i>Fe_{1.5}Zn_{0.5}VSb</i> |
| $N_{YZ} = 6$ e.g., Co $_a$ ScAl | <i>Co₂ScAl</i> | $3\alpha + 4\beta = 6$ <i>Co₂ScAl</i> | $3\alpha + 5\beta = 6$ <i>Co₂ScAl</i> | $3\alpha + 6\beta = 6$ <i>ZnScAl</i> <i>Co₂ScAl</i> | | $\alpha = -2$ | $\alpha - \beta = -2$ <i>Cu₂ScAl</i> | $\alpha - 2\beta = -2$ <i>Co_{0.67}Zn_{1.33}ScAl</i> |
| $N_{YZ} = 7$ e.g., Co $_a$ TiAl | <i>CoTiAl + Co₂</i> | $3\alpha + 4\beta = 5$ | $3\alpha + 5\beta = 5$ <i>CuTiAl</i> | $3\alpha + 6\beta = 5$ <i>Co_{0.33}Zn_{0.67}TiAl</i> | | $\alpha = -1$ | $\alpha - \beta = -1$ <i>Co_{0.5}Cu_{1.5}TiAl</i> | $\alpha - 2\beta = -1$ <i>CoZnTiAl</i> |
| $N_{YZ} = 8$ e.g., Co $_a$ VAl | <i>CoVAl + Co_{1.3}</i> | $3\alpha + 4\beta = 4$ <i>NiVAl</i> | $3\alpha + 5\beta = 4$ <i>Co_{0.5}Cu_{0.5}VAl</i> | $3\alpha + 6\beta = 4$ <i>Co_{0.67}Zn_{0.33}VAl</i> | | $\alpha = 0$ <i>Ni₂VAl</i> | $\alpha - \beta = 0$ <i>CoCuVAl</i> | $\alpha - 2\beta = 0$ <i>Co_{1.33}Zn_{0.67}VAl</i> |
| $N_{YZ} = 9$ e.g., Co $_a$ TiSb | <i>CoTiSb</i> | $3\alpha + 4\beta = 3$ <i>CoTiSb</i> | $3\alpha + 5\beta = 3$ <i>CoTiSb</i> | $3\alpha + 6\beta = 3$ <i>CoTiSb</i> | Good Semiconductor <i>XYZ</i> | $\alpha = 1$ | $\alpha - \beta = 1$ | $\alpha - 2\beta = 1$ |
| $N_{YZ} = 10$ e.g., Co $_a$ VSb | | $3\alpha + 4\beta = 2$ | $3\alpha + 5\beta = 2$ | $3\alpha + 6\beta = 2$ | Near Semiconductor <i>XYZ</i> Metal <i>XYZ</i> | $\alpha = 2$ <i>Co₂VSb</i> | $\alpha - \beta = 2$ <i>Co_{1.5}Cu_{0.5}TiSb</i> <i>Co₂VSb</i> | $\alpha - 2\beta = 2$ <i>Co_{1.67}Zn_{0.33}TiSb</i> <i>Co₂VSb</i> |

Figure 5. Relationship of the compositions α and β in the generic formulation $X_{\alpha}X'_{\beta}YZ$. The α - β relationship is subject to two constraints: ensuring the electron count is suitable for semiconductors (the relationship is indicated in red font) and maintaining an atomic concentration such that $1 \leq \alpha + \beta \leq 2$. The endpoints of half-Heuslers ($\alpha + \beta = 1$) and full-Heuslers ($\alpha + \beta = 2$) are shown in blue fonts. The hashed areas denote that α and β cannot fulfill a logical relation. The shaded elliptical areas highlight regions more likely to achieve good semiconductors according to density-functional-theory predictions. The first column provides examples of Fe- and Co-based systems, which can be generalized to include other elements.

5. Atomic occupation rules and Emerging weak metallicity

As intermetallic alloys, Heuslers are susceptible to structural complications such as occupational disordering [8,9], potentially exacerbated by partial filling in the off-stoichiometric systems. For instance, Fe_{1.5}TiSb was predicted to adopt a space group $R3m$ using the cluster expansion method (see Supplementary Materials) [18]. By contrast, our tetragonal model in Figure 2, which has a higher formation energy of 11 meV/atom, has been manually designed to facilitate the visualization of orbital characteristics. An intriguing question arises: to what extent can meta-stable structures reflect actual material attributes? Understanding the underlying principles is crucial for guiding theoretical predictions and interpreting experimental results. This section outlines several fundamental structural rules derived from our density-functional-theory calculations.

When discussing bandgap mechanisms, we have posited that the 4c sites are preferentially occupied prior to filling the 4d sites. This ordering principle, defined as the **4c's full occupation rule**, is strongly driven by the need to minimize Coulombic repulsion between the 4c and 4d sites. Following this, the 4d sites are then partially filled with atoms, resulting in numerous possible occupation patterns. An ordered distribution of atoms across the 4d sites, referred to as the **4d's ordered distribution rule**, is found energetically most favorable, as it further diminishes the 4c-4d repulsion. Moreover, if the 4c sites contain two different types of atoms, they are likely to be ordered mixed.

Quaternary $X_{\alpha}X'_{\beta}YZ$ is subject to an additional rule in arranging X and X' ions. For example, (Fe $_a$ Cu $_{\beta}$)TiSb can utilize both $s^2p^6d^{10}+\beta \times d^6$ and $s^2p^6d^{10}+\beta \times d^{10}$ mechanisms to form two types of semiconductors, each associated with distinct 4c-4d occupation patterns for the Fe and Cu atoms. This behavior is governed by the **4d's size selection rule**, which is motivated by the objective of harvesting energy from bandgap formation. To open a bandgap under the $s^2p^6d^{10}+\beta \times d^6$

mechanism, the 4d sites preferentially host larger ions to enhance 4c-4d interactions, thereby increasing the e_g - e_g orbital interaction (Figure 6a). Conversely, the $s^2p^6d^{10}+\beta\times d^{10}$ mechanism favors smaller ions at the 4d sites, keeping the d^{10} orbitals more compact and creating a gap from higher electronic states. Applying these principles to $(\text{Fe}_a\text{Cu}_\beta)\text{TiSb}$ [23], the $s^2p^6d^{10}+\beta\times d^6$ semiconductors require 4d sites occupied by the larger Fe, while the $s^2p^6d^{10}+\beta\times d^{10}$ semiconductors have their 4d sites filled with the smaller Cu ions.

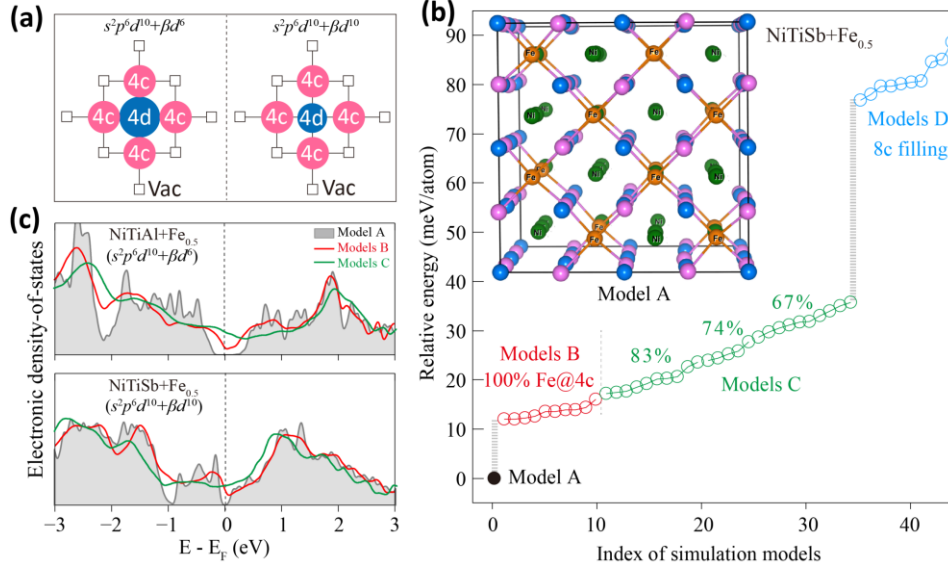


Figure 6. Occupation rules and consequences of deviation. (a) Sketch of the $4d$'s size selection rule designed to facilitate the semiconducting phase of quaternary $X_aX'_bYZ$. (b) Energy penalties associated with deviating from the occupation rules. The inset shows an ideal ground state, Model A, for $\text{NiTiSb}+\text{Fe}_{0.5}$. The structure is a $2\times 2\times 2$ supercell containing 112 atoms in total, including 32 Ni and 16 Fe atoms; while 16 Ni and 16 Fe atoms ordered fill all the 4c sites, the remaining 16 Ni atoms evenly occupy half of the 4d sites. Model B violates the $4d$'s ordered distribution rule, Model C breaches the $4d$'s size selection rule, and Model D also flouts the $4c$'s full occupation rule. Models B through D utilize larger supercells with 378 atoms to better account for occupation disorder. (c) Density-of-states for $\text{NiTiAl}+\text{Fe}_{0.5}$ and $\text{NiTiSb}+\text{Fe}_{0.5}$. For Models B and C, each result represents an average taken from many supercell structures.

While electron number rules can be rigorously enforced through composition control, adherence to occupation rules may be more challenging in practice. In this context, we explore the consequences of such violations in two Ni-based systems (Figure 6): $\text{NiTiAl}+\text{Fe}_{0.5}$ and $\text{NiTiSb}+\text{Fe}_{0.5}$, which follows the $s^2p^6d^{10}+\beta\times d^6$ and $s^2p^6d^{10}+\beta\times d^{10}$ mechanisms, respectively. To apply the atomic occupation rules, supercell models with $2\times 2\times 2$ unitcell size are constructed. The first two occupation rules can be readily implemented in this supercell, but applying the $4d$'s size selection rule presents certain complexities. In $\text{NiTiAl}+\text{Fe}_{0.5}$, all the larger Fe atoms are strategically placed in the 4d sites; in $\text{NiTiSb}+\text{Fe}_{0.5}$, all Fe atoms are placed in the 4c sites. Model A (see the inset of Figure 6b), which rigorously adheres to all the rules, exhibits semiconducting properties with bandgaps of 0.43 eV and 0.11 eV for $\text{NiTiAl}+\text{Fe}_{0.5}$ and $\text{NiTiSb}+\text{Fe}_{0.5}$, respectively (Figure 6c).

Any deviation from the ideal occupations destabilizes the structure, as demonstrated by the penalizing energies in $\text{NiTiSb}+\text{Fe}_{0.5}$ (Figure 6b). Violating the $4d$'s ordered distribution rule, likely under finite temperatures, results in the partial and random occupation of 4d sites by inadequate Ni atoms. This randomness, considered in larger supercells (Models B), leads to increased energies of at least 11 meV/atom and the emergence of weak metallicity (Figure 6c). Violations of the $4d$'s size selection rule occur as Fe atoms gradually fill 4d sites (Models C), progressing to a completely random mix of Fe and Ni (67% Fe remaining in 4c sites), which increases energy and enhances metallic behavior. Finally, the $4c$'s full occupation rule is violated when Fe and Ni mix randomly in all interstitial sites, transforming the 4c and 4d Wyckoff positions into a single 8c symmetry (Models D). These structures exhibit significantly higher energies and are energetically discontinuous from the earlier models.

6. Discussion and Perspective

This work focuses on $3d$ -electron transition-metal elements, including low-valent elements such as Sc, Ti, V, and Cr, and high-valent elements like Fe, Co, Ni, Cu, and Zn. The landscape could be readily extended to elements with $4d$ -electrons and further enriched by exploring other anionic elements and their mixtures [26]. In addition, Mn is excluded from this study for two primary reasons: firstly, Mn can occupy both the $4c$ and $4d$ tetrahedral sites and the $4b$ octahedral sites, introducing significant structural complexities, such as those seen in inverse Heuslers [4]. Secondly, Mn in the $4b$ sites typically exhibits strongly localized magnetic moments, leading to distinct magnetic and metallic behaviors.

A distinctive structural feature of the off-stoichiometric Heuslers is their capacity to tolerate high-energy configurations, such as the meta-stable structures arising from the atomic disordering (see Section 5). Further theoretical insights in $\text{Fe}_{1.5}\text{TiSb}$ are provided in the [Supplementary Material](#), which investigates the energetics and lattice dynamical stability. Regarding thermodynamic stability, we have demonstrated that the half-Heusler $(\text{Fe}_{0.67}\text{Cu}_{0.33})\text{TiSb}$ exhibits the lowest formation energy among the $(\text{Fe}_\alpha\text{Cu}_\beta)\text{TiSb}$ series, while a higher atomic filling reduces the thermodynamic stability [23]. Nevertheless, the limit stoichiometry of $\alpha + \beta = 2$ has been experimentally achieved in the $(\text{FeCu})\text{TiSb}$ sample, as shown in [Figure 4b](#).

While the well-established semiconductors (e.g., CoTiSb , NiTiSn , and Fe_2VAl) do not exhibit a magnetic degree of freedom, magnetic Heuslers are typically metals or half-metals. This observation underscores the strong interconnections between nonmagnetic semiconductors and magnetic metals, as well as the contrasting behaviors of magnetic semiconductors. Indeed, only a few exotic magnetic semiconductors have been theoretically proposed. For example, CoVTiAl is a ferromagnetic semiconductor [27], and CrVTiAl is a fully-compensated ferrimagnetic semiconductor [29], which embody these contradictory properties through the unique characteristics of the $\text{Al-}3p$ orbitals [27]. However, subsequent experiments on CrVTiAl have revealed gapless behaviors that deteriorate its semiconducting properties [30]. Overall, achieving a robust merger between magnetism and semiconductor properties in Heusler compounds remains an uncommon and rare occurrence. Based on these observations, we have employed spin-unpolarized simulations. While this assumption is valid for most materials, we indeed identify its limitations in some cases. For instance, we identify FeZnVAl as a semiconductor from the nonmagnetic simulations, aligning with a recent report [31]. However, spin-polarization is strongly favored in this material, effectively transforming it into a magnetic metal. Further research is underway to address the magnetic issue.

7. Summary

The vacancy-filling strategy, applied to the generic formula $\text{X}_\alpha\text{X}'_\beta\text{YZ}$ ($1 \leq \alpha + \beta \leq 2$), serves as a practical approach for expanding the range of semiconducting systems. This approach naturally encompasses the well-known integer-stoichiometric Heuslers and facilitates the prediction of numerous off-stoichiometric variants, thereby providing a comprehensive landscape of semiconducting Heusler compounds. The coefficients α and β are determined based on the valence electron counts that contribute to semiconductor properties, and the corresponding bandgap mechanisms are categorized into three types: $s^2p^6d^{10}$, $s^2p^6d^{10+\beta} \times d^6$, and $s^2p^6d^{10+\beta} \times d^{10}$. Materials that satisfy bandgap mechanisms, which determine the necessary electron counts for the semiconducting behavior, are also subject to practical electronic and structural constraints to develop bandgaps. For example, atomic occupation patterns are crucial in determining the material properties: ideal site occupancy typically results in effective semiconducting behavior, whereas occupation disorder can lead to weak metallicity. Despite their considerable complexity in composition and site occupation, these materials can be effectively characterized by simple rules, summarized as follows.

Electron number rules for designing semiconducting Heuslers. (1) Integer-stoichiometric Heuslers: Half-Heuslers, represented by the generic formula $\text{X}_\alpha\text{X}'_\beta\text{YZ}$ with $\alpha + \beta = 1$, open their bandgaps through the $s^2p^6d^{10}$ mechanism, resulting in 18 valence electrons. For full-Heuslers, the ternary systems rely on the $s^2p^6d^{10+\beta} \times d^6$ bandgap mechanism and have 24 electrons, while the quaternary systems utilize the $s^2p^6d^{10+\beta} \times d^{10}$ mechanism and have 28 electrons. **(2) Vacancy-filling off-stoichiometric Heuslers** with $1 < \alpha + \beta < 2$: The bandgap mechanisms are either $s^2p^6d^{10+\beta} \times d^6$ or $s^2p^6d^{10+\beta} \times d^{10}$. While the electron counts in ternary systems are fixed at a few discrete values, they vary continuously from 18 to 28 in

quaternary systems. **(3) Good semiconductors** typically have compositions proximate to half-Heuslers. Elevated atomic concentrations and electron counts can lead to a reduction or closure of the bandgap.

Site occupation rules for deriving low-energy semiconductors. **(1) 4c's full occupation rule:** Despite the geometrical symmetry between 4c and 4d sites, atoms have a pronounced priority to first fill the 4c sites before entering the 4d sites. Violating this propensity requires overcoming a high energy barrier. **(2) 4d's ordered distribution rule:** If the 4d sites are partially occupied, the ordered distribution of the filling atoms is energetically favorable. This rule also applies to 4c sites when accommodating more than one element. Breaking this rule requires less energy than the previous rule. **(3) 4d's size selection rule:** Larger ions are favored at the 4d sites under the $s^2p^6d^{10}+\beta\times d^6$ mechanism, whereas smaller ions are preferred when the $s^2p^6d^{10}+\beta\times d^{10}$ mechanism is employed. Deviations can lead to the emergence of weak metallic behaviors.

Acknowledgments

This work was supported by the Natural Science Foundation of China (52272226 and 11904156).

Conflict of Interest

The authors declare no conflict of interest.

Data Availability Statement

The data supporting this study's findings are available from the corresponding author upon reasonable request.

References

- [1] Friedrich Heusler, *Über magnetische manganlegierungen*. *Verh. Dtsch. Phys. Ges.* **5**, 219 (1903).
- [2] I. Galanakis, P. H. Dederichs, N. Papanikolaou, *Origin and properties of the gap in the half-ferromagnetic Heusler alloys*. *Physical Review B*. **66**, (2002).
- [3] I. Galanakis, P. H. Dederichs, N. Papanikolaou, *Slater-Pauling behavior and origin of the half-metallicity of the full-Heusler alloys*. *Physical Review B*. **66**, 174429 (2002).
- [4] S Skaftouros, Kemal Özdoğan, E Şaşıoğlu, I Galanakis, *Generalized Slater-Pauling rule for the inverse Heusler compounds*. *Physical Review B*. **87**, 024420 (2013).
- [5] Linus Pauling, *The Nature of the Interatomic Forces in Metals*. *Physical Review*. **54**, 899 (1938).
- [6] J. C. Slater, *The Ferromagnetism of Nickel. II. Temperature Effects*. *Physical Review*. **49**, 931 (1936).
- [7] Kemal Özdoğan, E Şaşıoğlu, I Galanakis, *Slater-Pauling behavior in LiMgPdSn-type multifunctional quaternary Heusler materials: Half-metallicity, spin-gapless and magnetic semiconductors*. *Journal of Applied Physics*. **113**, (2013).
- [8] KP Bhatti, V Srivastava, DP Phelan, RD James, C Leighton, *Heusler Alloys: Properties, Growth, Applications*. 2016, Springer.
- [9] Tanja Graf, Claudia Felser, Stuart S. P. Parkin, *Simple rules for the understanding of Heusler compounds*. *Progress in Solid State Chemistry*. **39**, 1 (2011).
- [10] Sheron Tavares, Kesong Yang, Marc A Meyers, *Heusler alloys: Past, properties, new alloys, and prospects*. *Progress in Materials Science*. **132**, 101017 (2023).
- [11] Shashwat Anand, Max Wood, Yi Xia, Chris Wolverton, G. Jeffrey Snyder, *Double Half-Heuslers*. *Joule*. **3**, 1226 (2019).
- [12] Zihang Liu, Shuping Guo, Yixuan Wu, Jun Mao, Qing Zhu, Hangtian Zhu, Yanzhong Pei, Jiehe Sui, Yongsheng Zhang, Zhifeng Ren, *Design of high-performance disordered half-Heusler thermoelectric materials using 18-electron rule*. *Advanced Functional Materials*. **29**, 1905044 (2019).
- [13] Airan Li, Madison K Brod, Yuechu Wang, Kejun Hu, Pengfei Nan, Shen Han, Ziheng Gao, Xinbing Zhao, Binghui Ge, Chenguang Fu, *Opening the bandgap of metallic Half-Heuslers via the introduction of d-d orbital interactions*. *Advanced Science*. **10**, 2302086 (2023).

- [14] Wolfgang G. Zeier, Shashwat Anand, Lihong Huang, Ran He, Hao Zhang, Zhifeng Ren, Chris Wolverton, G. Jeffrey Snyder, *Using the 18-Electron Rule To Understand the Nominal 19-Electron Half-Heusler NbCoSb with Nb Vacancies*. *Chemistry of Materials*. 29, 1210 (2017).
- [15] Shashwat Anand, Kaiyang Xia, Vinay I. Hegde, Umut Aydemir, Vancho Kocovski, Tiejun Zhu, Chris Wolverton, G. Jeffrey Snyder, *A valence balanced rule for discovery of 18-electron half-Heuslers with defects*. *Energy & Environmental Science*. 11, 1480 (2018).
- [16] Jiangang He, S. Shahab Naghavi, Vinay I. Hegde, Maximilian Amsler, Chris Wolverton, *Designing and Discovering a New Family of Semiconducting Quaternary Heusler Compounds Based on the 18-Electron Rule*. *Chemistry of Materials*. 30, 4978 (2018).
- [17] Runan Xie, Jean-Claude Crivello, Céline Barreteau, *Screening New Quaternary Semiconductor Heusler Compounds By Machine-Learning Methods*. *Chemistry of Materials*. 35, 7615 (2023).
- [18] N. Naghibolashrafi, S. Keshavarz, Vinay I. Hegde, A. Gupta, W. H. Butler, J. Romero, K. Munira, P. LeClair, D. Mazumdar, J. Ma, A. W. Ghosh, C. Wolverton, *Synthesis and characterization of Fe-Ti-Sb intermetallic compounds: Discovery of a new Slater-Pauling phase*. *Physical Review B*. 93, 104424 (2016).
- [19] A. Tavassoli, A. Grytsiv, G. Rogl, V. V. Romaka, H. Michor, M. Reissner, E. Bauer, M. Zehetbauer, P. Rogl, *The half Heusler system $Ti_{1+x}Fe_{1.33-x}Sb-TiCoSb$ with Sb/Sn substitution: phase relations, crystal structures and thermoelectric properties*. *Dalton Trans.* 47, 879 (2018).
- [20] Shashwat Anand, G. Jeffrey Snyder, *Structural Understanding of the Slater-Pauling Electron Count in Defective Heusler Thermoelectric $TiFe_{1.5}Sb$ as a Valence Balanced Semiconductor*. *ACS Applied Electronic Materials*. 4, 3392 (2022).
- [21] Luyao Wang, Zirui Dong, Shihua Tan, Jiye Zhang, Wenqing Zhang, Jun Luo, *Discovery of a Slater-Pauling Semiconductor $ZrRu_{1.5}Sb$ with Promising Thermoelectric Properties*. *Advanced Functional Materials*. 32, 2200438 (2022).
- [22] Zirui Dong, Jun Luo, Chenyang Wang, Ying Jiang, Shihua Tan, Yubo Zhang, Yuri Grin, Zhiyang Yu, Kai Guo, Jiye Zhang, Wenqing Zhang, *Half-Heusler-like compounds with wide continuous compositions and tunable p- to n-type semiconducting thermoelectrics*. *Nature Communications*. 13, 35 (2022).
- [23] Weimin Hu, Song Ye, Qizhu Li, Binru Zhao, Masato Hagihala, Zirui Dong, Yubo Zhang, Jiye Zhang, Shuki Torri, Jie Ma, Binghui Ge, Jun Luo, *Strategic Design and Mechanistic Understanding of Vacancy-Filling Heusler Thermoelectric Semiconductors*. *Advanced Science*. 11, 2407578 (2024).
- [24] Jiajun Chen, Zirui Dong, Qizhu Li, Binghui Ge, Jiye Zhang, Yubo Zhang, Jun Luo, *Enhanced Thermoelectric Performance in Vacancy-Filling Heuslers due to Kondo-Like Effect*. *Advanced Materials*. 36, 2405858 (2024).
- [25] Siyuanyang Yin, Qizhu Li, Shaoqin Wang, Jiajun Chen, Zirui Dong, Yubo Zhang, Binghui Ge, Jiye Zhang, Jun Luo, *Structure and thermoelectric properties of half-Heusler-like $TiFeCuxSb$ alloys*. *Journal of Materiomics*. 10, 523 (2024).
- [26] Hui Huang, *Synthesis and thermoelectric properties of defective Heusler-based compounds*. 2021, University of Chinese Academy of Sciences.
- [27] I Galanakis, Kemal Özdoğan, E Şaşıoğlu, *A proposal for an alternative class of spin filter materials: Hybridization-induced high-TC ferromagnetic semiconductors $CoVXAl$ ($X= Ti, Zr, Hf$)*. *Applied Physics Letters*. 103, 142404 (2013).
- [28] Yurong Ruan, Tao Feng, Ke Zhong, Bing Wen, Wenqing Zhang, *Full-shell d-orbitals of interstitial Ni and anomalous electrical transport in Ni-based half-Heusler thermoelectric semiconductors*. *Materials Today Physics*. 48, 101558 (2024).
- [29] I Galanakis, Kemal Özdoğan, E Şaşıoğlu, *High-T C fully compensated ferrimagnetic semiconductors as spin-filter materials: The case of $CrVXAl$ ($X= Ti, Zr, Hf$) Heusler compounds*. *Journal of Physics: Condensed Matter*. 26, 086003 (2014).
- [30] Gregory M Stephen, Christopher Lane, Gianina Buda, David Graf, Stanislaw Kaprzyk, Bernardo Barbiellini, Arun Bansil, Don Heiman, *Electrical and magnetic properties of thin films of the spin-filter material $CrVTiAl$* . *Physical Review B*. 99, 224207 (2019).
- [31] Abhigyan Ojha, Rama Krushna Sabat, Sivaiah Bathula, *Exploring the thermoelectric performance of $NiFeMnAl$ and $ZnFeVAl$ as novel quaternary Heusler compounds*. *Materials Science and Engineering: B*. 311, 117789 (2025).